Autoionization and isotope effect in the threshold photoelectron spectrum of 12CO2 and 13CO2

Tomas Baer and Paul M. Guyon

Citation: J. Chem. Phys. **85**, 4765 (1986); doi: 10.1063/1.451736
View online: http://dx.doi.org/10.1063/1.451736
View Table of Contents: http://jcp.aip.org/resource/1/JCPSA6/v85/i9
Published by the American Institute of Physics.

Autoionization and isotope effect in the threshold photoelectron spectrum of $^{12}CO_2$ and $^{13}CO_2$

Tomas Baer [a] and Paul M. Guyon[b]
LURE, Universite de Paris-sud, 91405 Orsay, France

(Received 23 December 1985; accepted 22 July 1986)

Threshold photoelectron spectra of $^{12}CO_2$ and $^{13}CO_2$ have been obtained from the onset at 900 Å (13.75 eV) to 620 Å (20 eV) at a 9 meV resolution using dispersed synchrotron radiation with a 0.3 Å bandpass. A number of forbidden and/or previously unobserved transitions have been assigned for the $\tilde{X}$, $\tilde{A}$, $\tilde{B}$, and $\tilde{C}$ states of CO_2^+. Photoelectron spectra by electron time of flight at selected excitation wavelengths in the Franck–Condon gap region below the $\tilde{A}$ state, reveal the autoionization of neutral valence states as well as Rydberg series converging to the $\tilde{A}\,^2\Pi_u$ and $\tilde{B}\,^2\Sigma_u^+$ states. The photoelectron energy distribution obtained upon excitation of the Rydberg states is consistent with that given by the Bardsley–Smith model for autoionization, while the superexcited valence states decay via a resonance autoionization process proposed previously by Guyon, Baer, and Nenner. These valence states are also responsible for the strong enhancement of vibrationally forbidden transitions, such as (000) → (010). Finally, several threshold electron peaks in the region between the $\tilde{A}$ and $\tilde{C}$ states, whose origin can be attributed to autoionization, are shown to be highly sensitive to isotopic substitution.

I. INTRODUCTION

A number of careful studies of the photoelectron spectrum of CO_2 have been reported during the past few years.[1–7] Yet another such investigation surely requires some justification. The present study builds on and differs from the previous work in a number of ways. First of all, four of the previous high resolution PES investigations were done by using He(I) or Ne(I) lamps in which the ejected electrons were energy analyzed.[1–4] Three others used the technique of threshold photoelectron spectroscopy (TPES).[5–7] In this approach, the electron analyzer is tuned to pass only zero energy electrons while the photon monochromator wavelength is varied. This threshold technique which scans through the rich absorption spectrum can also form via autoionization ion states that are not produced in the fixed wavelength photoelectron spectroscopy using the higher energy radiation of the He(I) and Ne(I) lamps.

In the present work, we report on the TPES of CO_2 not only in the vicinity of the major electronic states, but also in the Franck–Condon gap regions between the $\tilde{X}$ and $\tilde{A}$, and $\tilde{B}$ and $\tilde{C}$ states. In addition, we have investigated the ^{13}C isotope of CO_2. Although the isotope shift in the vibrational levels is small, it is observable and is extremely useful in aiding the identification of the vibrational bands.

The PES of the ground electronic state of CO_2^+ is complex because of vibronic perturbations. Although only symmetric vibrations are generally excited in PES, a Renner–Teller interaction in the doublet $^2\Pi\tilde{X}$ vibronic state causes the (010) vibration to be excited.[1,3–5] The intensity of this band is further increased in the TPES presumably as a result of the contribution of autoionizing bent neutral valence states. The enhancement of certain peak intensities by the autoionizing channels and the vibronic interactions makes the analysis of the ground state of CO_2^+ extremely challenging.

The $^2\Pi_g\tilde{X}$ and $^2\Pi_u\tilde{A}$ states are separated by over 3 eV. A large number of autoionizing Rydberg states converging to the $\tilde{A}$ and $\tilde{B}$ ionic states are evident in both the absorption spectrum as well as the photoionization efficiency (PIE) spectrum. Some of these have been assigned while the origin of others remains a mystery. A precise knowledge of the energy is certainly essential in assigning these peaks, but this information is often insufficient when the absorption spectrum is congested and perturbed. In these situations, excitation spectra of specific decay channels, such as the threshold electron spectra or constant final ionic state spectra, are of help since they reveal the series principally coupled to that channel. Complementary information can thus be obtained from photoelectron spectra at selected photon energies.

The earlier studies of Frey *et al.*[5] and Batten *et al.*[7] indicated the presence of a number of sharp TPES peaks in the region of the $\tilde{A}$ state that could not be attributed to the major ($v_1$00) progression observed in the H(I) PES. Because of the sharp autoionizing transitions in this region, it was difficult in these previous investigations to determine whether the origin of these extra TPES peaks were the result of insufficient suppression of energetic electrons, and therefore merely reflected the autoionization structure, or whether they resulted from real threshold electron peaks and corresponded to ion states with energies equal to the photon energy.

II. EXPERIMENTAL APPROACH

CO_2^+ ions were formed by passing a beam of dispersed synchrotron radiation from the ACO storage ring (LURE)

[a] Permanent address: Department of Chemistry, University of North Carolina, Chapel Hill, North Carolina 27514.
[b] Laboratorire des Collision Atomiques et Moleculaires, Bat. 351, Universite de Paris-sud, 91405 Orsay, France.

 0021-9606/86/214765-14$02.10

through a cell containing CO_2 gas at a pressure of about 10^{-3} Torr. The synchrotron light was dispersed by a 1 m McPherson, normal incidence monochromator equipped with a 3600 lines/mm holographic grating. Slit widths of 100 μm yielded a photon resolution of about 0.3 Å which translates to an energy resolution of 5 meV at 900 Å and 12 meV at 600 Å.

Two types of photoelectron spectra were collected in this study. In the normal PES, the photon energy remains fixed and the distribution of electron energies is collected. This was done by measuring the electron time-of-flight (TOF) distribution following the ionization by the 1.5 ns (FWHM) wide synchrotron radiation pulse. The other type of PES is called threshold photoelectron spectroscopy (TPES) in which only zero energy electrons are collected while the photon energy is scanned across the various ionic states.

A. Threshold photoelectron spectra (TPES)

The threshold photoelectron spectrum is a scan of nominally zero energy electrons vs photon energy and thus represents a zero electron energy excitation spectrum. The zero energy electrons were collected by a combination of discrimination against energetic electrons on the basis of their angular dispersion and their time of flight. This technique has been described in a previous publication,[8] and recently improved by the use of a longer electron drift tube. Figure 1 shows the photoionization region employed for this purpose. The electron acceleration and drift distance was 4.5 cm. In order to collect the electrons produced by a photon pulse prior to the onset of the subsequent photon pulse, it was necessary to accelerate the electrons to 4 V. This yielded a zero energy electron TOF of 50 ns which is less than the 73.5 ns between photon pulses.

An example of the resolution achieved by this arrangement is shown in Fig. 2 in which the TPES of Ar is displayed. Of particular interest is the resolution of 9 meV and the nearly complete suppression of the strong autoionization peaks in between the two spin orbit states of Ar^+. In this TPES spectrum and those of $^{12}CO_2$ to be presented, the data were acquired at 0.1 Å/point for a collection time of 4 to 8 s/point. Typical count rates at the TPES peaks were 1000 c/s. The $^{13}CO_2$ scan was acquired at intervals of 0.2 Å/point.

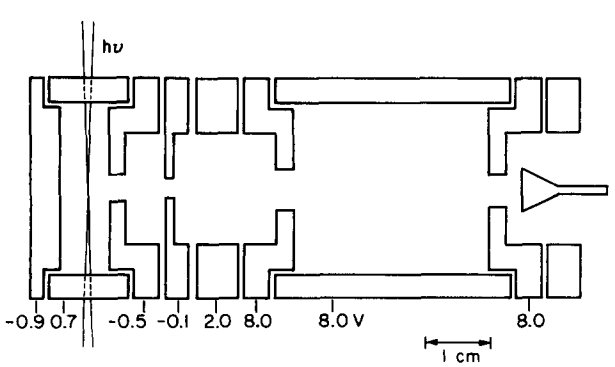

FIG. 1. The ionization region and electron time-of-flight arrangement with the indicated applied voltages. The whole spectrometer is magnetically shielded by a double μ metal shield. This setup was adapted from the experiment of Field *et al.* (Ref. 9).

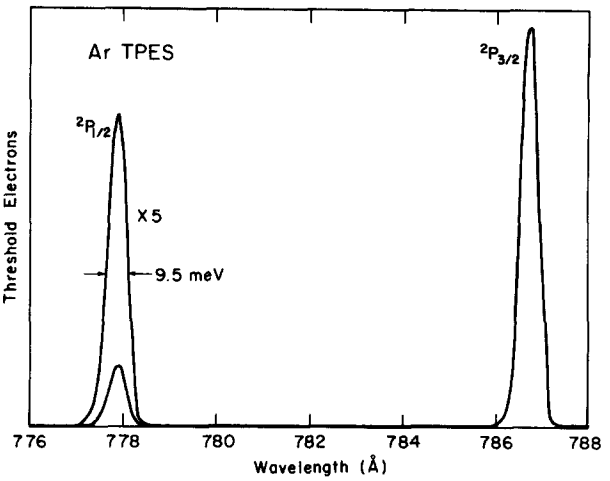

FIG. 2. The threshold photoelectron spectrum (TPES) of Ar under the conditions of the CO_2 experiment.

B. PES by electron time of flight

The PES at fixed photon energies were collected by using the electron signal as start and the delayed sychrotron light pulse as stop inputs to a LeCroy QVt time to digital converter, the output of which was read by a Tektronix 4051 microcomputer. Energetic electrons ejected perpendicular to the electron extraction voltage hit the walls or apertures and are lost while electrons initially ejected along the experimental axis either toward or away from the electron detector arrive earlier or later than the zero energy electrons. The useful part of the electron TOF is the one to the short time-of-flight side of the zero energy electrons, that is the TOF of the electrons initially ejected toward the electron detector.

The electron flight time is a function of the initial electron energy and the voltages applied to the various plates in the electron acceleration and drift regions. The electron energy resolution is excellent at low energies but deteriorates rapidly at higher energies. In order to improve this resolution, some of the PES were obtained by applying a retarding potential in the ion source, thereby slowing down the energetic electrons. Of course, the zero energy electrons could not be detected under these conditions.

The energy to TOF conversion and the collection efficiencies for various electron energies were determined by photoionizing Ar at various photon energies above its ionization potential.

III. RESULTS AND ANALYSIS

Figure 3 shows the complete threshold photoelectron spectrum (TPES) and the photoionization efficiency (PIE) spectrum of $^{12}CO_2$ from the onset at 906 to 620 Å. From this complete scan, as well as several additional and shorter scans, it was possible to obtain a consistent set of energies for the various electronic states of $^{12}CO_2^+$. These are listed and compared with previous values in Table I. In addition, the values for $^{13}CO_2^+$ are also shown.

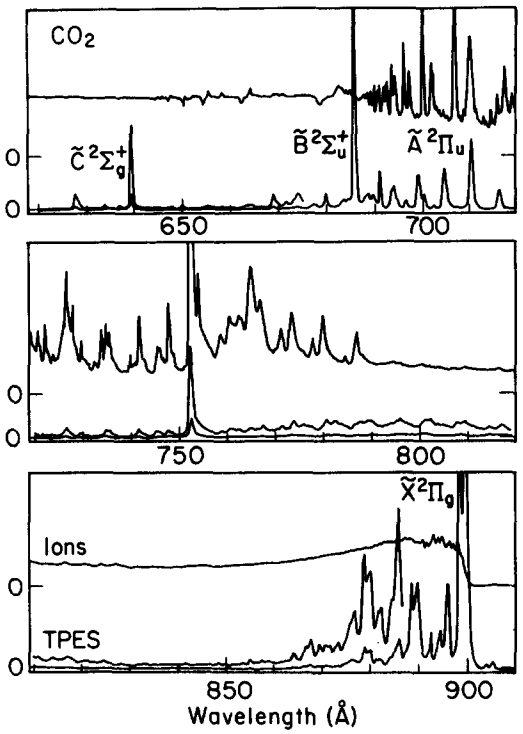

FIG. 3. The TPES and photoionization efficiency (PIE) spectrum of $^{12}CO_2$ from 900 to 620 Å.

The TPES of $^{12}CO_2$ shows the vibrational structure of the four electronic states, $\tilde{X}\,^2\Pi_g$, $\tilde{A}\,\Pi_u$, $\tilde{B}\,^2\Sigma_u^+$, and $\tilde{C}\,^2\Sigma_g^+$. In addition, there is a broad band with a maximum at about 800 Å, on which is superimposed a series of more or less regular peaks. This band is not observed in the He(I) PES. A similar, but less extensive, band is also seen below 640 Å. These bands lie in the Franck–Condon gaps between the $\tilde{X}$ and $\tilde{A}$, and $\tilde{B}$ and $\tilde{C}$ states, respectively. In the following sections, we analyze each of these bands in turn.

A. $\tilde{X}\,^2\Pi_g$ state

The vibrational spectrum of CO_2^+ in the ground electronic state is complicated because of the vibronic interaction between the two electronic spin orbit states $\Omega = 1/2$ and $\Omega = 3/2$ with bending vibrations of CO_2^+. This Renner–Teller interaction has the effect of splitting each of the degenerate $(0v_20)$ states into $2(v_2 + 1)$ states.[14] In addition, some of the states of similar energy and symmetry, such as the (100) and (020) levels, interact with each other via Fermi resonances thereby further complicating the spectral assignments.

Expanded TPES of the $\tilde{X}$ states of $^{12}CO_2^+$ and $^{13}CO_2^+$ are shown in Fig. 4. All of the spectra shown in this paper are unsmoothed and plotted by straight line connections between adjacent points. In order to compare the two spectra, the $^{13}CO_2$ TPES has been shifted toward longer wavelengths by 0.156 Å. This shift aligns the ground state of the two ions. Because the wavelength is inversely proportional to the energy, shifting the wavelength scale is not precisely correct. However, over the range between 900 and 870 Å the error is only 0.2 meV (2 cm^{-1}), clearly negligible compared to our accuracy in determining peak positions which is about $\pm$ 10 cm^{-1}. The shift of 0.156 Å (19 cm^{-1}) is just the difference in the ionization potential of the two molecules which arises from the difference in the zero point vibrational energies of the two isotopes. The three fundamental normal modes for the CO_2 molecule and CO_2^+ ion are known and listed in Table I. For a linear molecule of the type OCO, the ν_1 symmetric stretch, in which the central carbon atom remains fixed, has no isotopic shift, while the ν_2 and ν_3 modes are shifted according to the factor[14]

$$\rho = \sqrt{\frac{(m_c^* + 2m_0)m_c}{(m_c + 2m_0)m_c^*}} = 0.9716\,. \qquad (1)$$

This factor leads to a predicted I. P. shift of 14.5 cm^{-1}, which is within the experimental error of our measurement.

A number of the peaks in the TPES of $^{12}CO_2$ and $^{13}C_2$ are considerably more intense than observed in the previously published PES. For instance the hot bands, which are formed by the ionization of CO_2 molecules excited thermally to the (010) states, are clearly evident. The intensity, 2.5% of the (000) peak, is nearly equal to the Boltzman factor at 300 K of 3.7%. Yet, the (010) → (000) transition is strictly forbidden because the symmetry goes from odd to even. In-

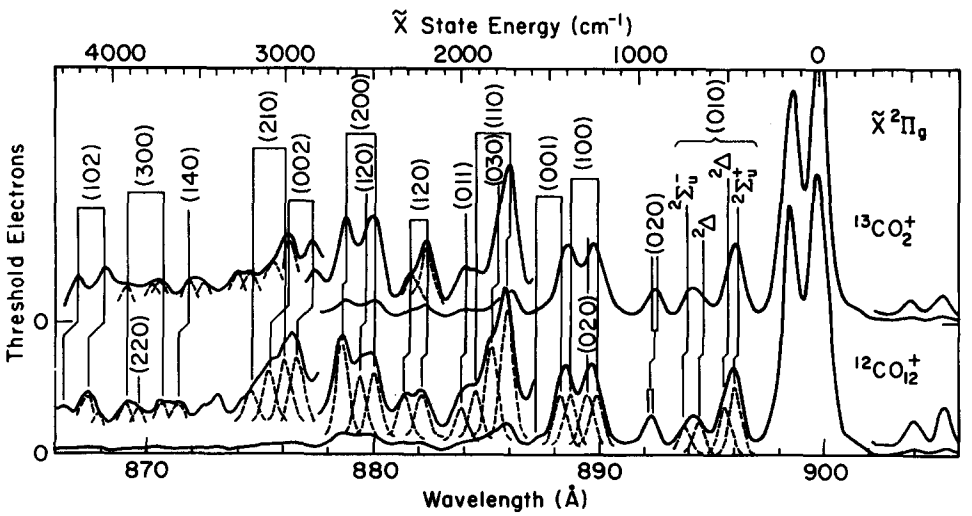

FIG. 4. The TPES of $^{12}CO_2$ and $^{13}CO_2$ in the region of the $\tilde{X}\,^2\Pi_g$ state. The $^{13}CO_2$ TPES has been shifted by 0.16 Å to lower wavelengths in order to superimpose the ionization energies of the two isomers.

TABLE I. Ionization potentials and vibrational frequencies of $^{12}CO_2^+$ and $^{13}CO_2^+$.

	I. P. (eV)	A (cm^{-1})[a]	ν_1 (cm^{-1})	ν_2 (cm^{-1})	ν_3 (cm^{-1})	Reference
$\tilde{X}\,^1\Sigma_g$ CO_2	...	...	1388	667 (648)[b]	2349 (2282)	10
$\tilde{X}\,^2\Pi_g$ CO_2^+	13.779	154	1230 (1225)[b]	519 (503)	1475 (1432)	This work
	13.776	137	1266	508	1472	3
	13.777	159	1240	508	...	5
	13.776	169	1299	492	...	7
	13.776	153	1250	484	1460	1
	...	160	1280	520	...	4
	...		1280 (1253)	513	1469	11
	13.769					13
$\tilde{A}\,^2\Pi_u$ CO_2^+	17.311	95	1115 (1113)	466 (454)	...	This work
	17.315	73	1118	467	...	3
	17.311	86	1110	...	...	5
	17.310	...	1121	...	...	7
	...	81	1145	484	...	1
	17.311[c]	96	1126	460	...	11
	...	70	1120	480	...	4
	17.312					13
$\tilde{B}\,^2\Sigma_u^+$	18.074		1270 (1272)	...	1820 (1775)	This work
	18.076	...	1279	...	2365	3
	18.068	...	1280	...	...	5
	18.076	...	1274	...	...	7
	...		1310	590	...	4
	...		1282	556	1855	2
	18.076			558		11
	18.077		1274			13
$\tilde{C}\,^2\Sigma_g^+$	19.387		1400 (1400)	625 (610)	1530 (1475)	This work
	19.388		1402	649	2345	3
	19.386		...	...	...	5
	19.386		1400	600	2960	4
	19.395		1347	580	1524	1
	19.395					7

[a] Spin-orbit energy.
[b] Values in parentheses refer to $^{13}CO_2$.
[c] Obtained from $\tilde{A} \rightarrow \tilde{X}$ fluorescence and CO_2 I. P. of 13.777 eV.

deed, this hot band is not observed in either the He(I)[1–4] or Ne(I)[3] PES, indicating that it gains its intensity through autoionizing channels. The hot bands are split by the formation of the ion in the two spin orbit states. The splitting determined from these hot band peaks is 164 cm^{-1}, which is within the experimental error (10 cm^{-1}) equal to the splitting of 156 cm^{-1} measured from the two vibrational ground state peaks.

Another set of very intense peaks is the (010) quartet. In the He(I) PES of Reineck *et al.*[1] their intensity is 1.5% of the (000) peaks, while in the Ne(I) PES of Potts and Fattahallah[3] the intensity is 4%. In Fig. 4 this same intensity is 26% of the (000) peaks. On the other hand, the allowed (100) peaks have about the same intensity (25%) in both the PES and the TPES. This enhanced intensity of the bending modes in the TPES may reflect the participation of bent valence or dissociative states in the autoionizing process. Such a suggestion has already been advanced previously by McCulloh[15] and Krauss *et al.*[16] on the basis of the broad and nearly structureless peak in the threshold region of the PI spectrum (900–860 Å in Fig. 3). The absorption spectrum, measured by Gentieu and Mentall,[17] has a similar shape but a cross section about twice as high as the PIE yield. The difference between the absorption and ionization cross section represents the yield of neutral products, which in the absence of molecular fluorescence is just the dissociation cross section. How this competition between dissociation and ionization produces ion states not normally observed in PES is discussed in more detail in Sec. III B 2.

The spectrum of the $\tilde{X}$ state is very congested. The only peak that may be considered as a single state results from the transition to the quasidegenerate (020) level at about 900 cm^{-1}. This has a Gaussian shape with a width of 10 meV (85 cm^{-1}) which is approximately the resolution of 9 meV as measured on the Ar TPES. All of the other peaks are much broader than our resolution. For this reason the major peaks, or clusters of peaks, have been deconvoluted using the minimum number of 10 meV wide Gaussian peaks necessary to describe the particular clusters. This deconvolution was carried out by comparing the sums of calculated 9 meV Gaussians of varying intensities and positions with the experimental peaks.

Most of the assignments in Fig. 3 have been derived from those of previous workers as well as from the extensive calculations of Gauyacq *et al.*[11] and the thesis work of Larcher.[12] The new assignments, especially in the higher energy region, have been aided by the comparison between the $^{12}CO_2^+$ and the $^{13}CO_2^+$ vibrational peaks. It is evident that a

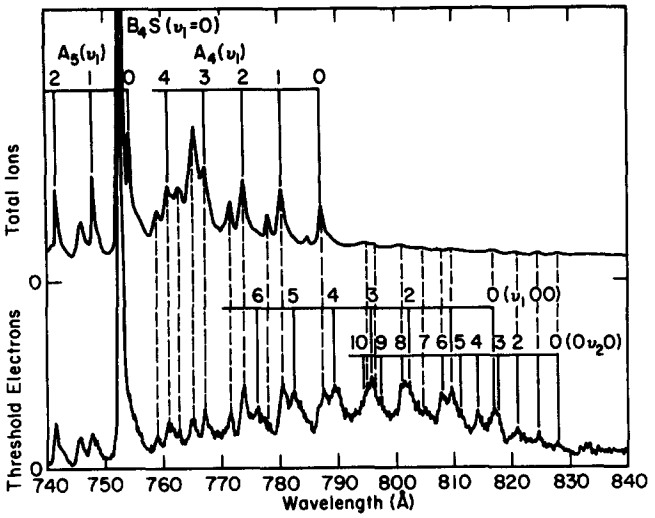

FIG. 5. The $^{12}CO_2$ TPES and PIE in the Franck–Condon gap region between the $\tilde{X}$ and $\tilde{A}$ states.

number of peak clusters are quite different in the $^{12}CO_2^+$ and $^{13}CO_2^+$ TPES. This is particularly so for all of the peaks above 1500 cm^{-1}. It is only the ($v_1$00) peaks that remain the same, as indeed they should. Because many of the states are a result of combination bands, assigning the peaks was done by applying the isotope shift only to the portion contributed by the ν_2 and the ν_3 modes. Thus the expected shift for the (110) peaks at 1740 and 1920 cm^{-1} is only 14 cm^{-1}, while the (030) peak of about the same energy is predicted to shift by 51 cm^{-1} thereby causing it to disappear under the (110) peak in the $^{13}CO_2$ spectrum. The higher energy transitions such as the $^{12}CO_2^+$ (002) peaks at 2930 and 3090 cm^{-1} as well as the (102) peaks at 4146 and 4310 cm^{-1} have experimentally observed shifts of 67, 85, 78, and 80 cm^{-1}, respectively. These are close to the predicted shift of 86 cm^{-1}. Exact agreement is not expected because perturbations of these states by nearby levels can shift the peaks in one direction or another.

B. The Franck–Condon gap between 840 and 740 Å

Figure 5 shows the TPES and the PIE of $^{12}CO_2$ in the region of 840 to 740 Å. Many of the threshold electron peaks are easily correlated with the strong autoionization peaks between 790 and 740 Å that have been previously identified as autoionizing peaks belonging to Rydberg states that converge to the $\tilde{A}$ and $\tilde{B}$ states of CO_2^+.[13,15] In the total ion scan, these peaks are in sharp contrast to the much weaker autoionizing peaks between 830 and 770 Å, which are barely visible. Yet, the relative intensities are very different in the TPES scan. While the strong autoionizing peaks give rise to some threshold electrons, it is evident that the TPES is much richer and more intense in the region of the very weak autoionization. As a result, the overall shape of the TPES band is very different from the shape of the PIE in this region. These two types of series autoionize by two different mechanisms, which will be described below.

1. Autoionization of sharp Rydberg states (740 to 790 Å): Direct autoionization

We have investigated a few of the strong $\tilde{A}$ state Rydbergs between 790 and 730 Å by measuring the distribution of electron energies that result when they are excited. These PES were obtained by electron time-of-flight analysis as described in the experimental section. However, for this experiment, we were interested in increasing the energy resolution for the higher energy electrons. Thus, the electrons were decelerated by about 0.2 eV. As a result, the initially zero energy electrons were suppressed and the electron energy range went from 0.2 to 3 eV. Under these conditions, the electron transmission as a function of the energy is nearly constant. These data for a number of the $\tilde{A}$ state Rydbergs are shown in Fig. 6 while the PES following excitation of the large $\tilde{B}$ ($v = 0$) Rydberg state at 752.2 Å is shown in Fig. 7. In all of the PES, it is evident that a number of vibrations are excited in the ground electronic CO_2^+ state. This is particularly evident when the spectra are compared with the one in Fig. 7(b) which is from a valley in between two autoionizing

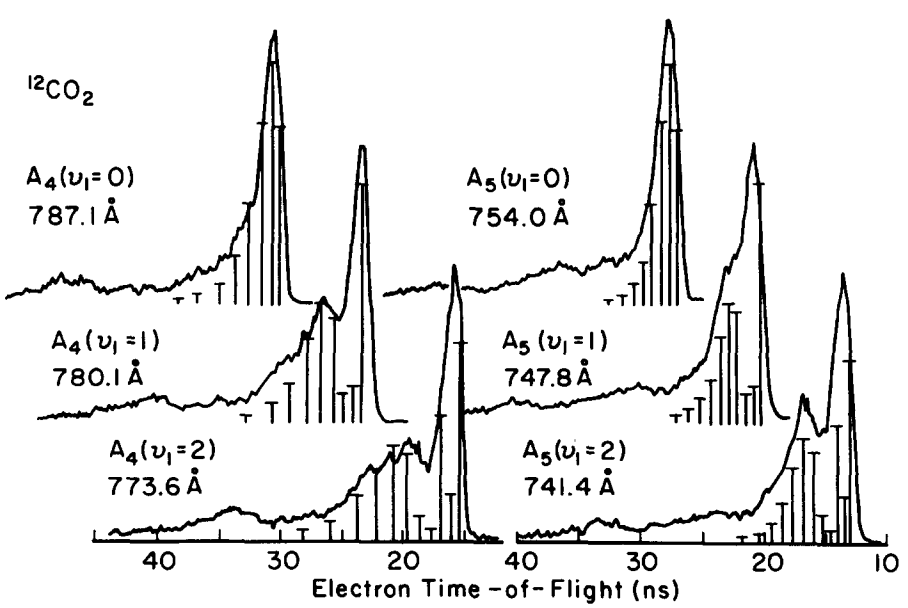

FIG. 6. Electron TOF distributions following excitation of several R_4 Rydberg states with various excitations in ν_1. The height of the vertical lines are proportional to the Franck–Condon factor between the Rydberg and ionic $\tilde{X}$ states. [See Eq. (2) in the text.]

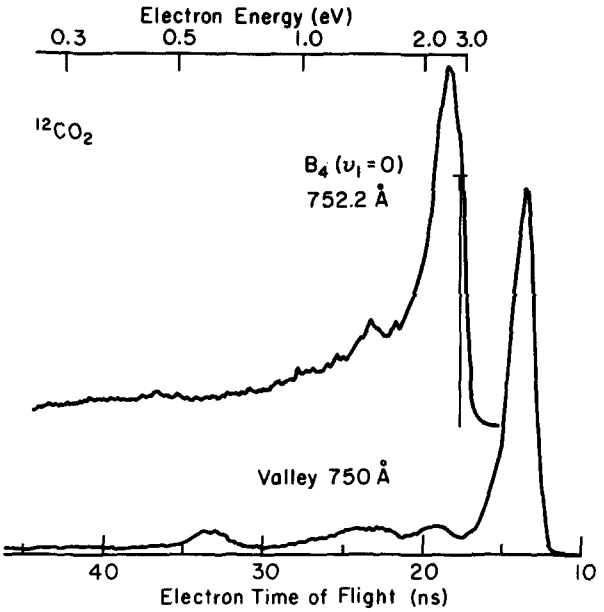

FIG. 7. Electron TOF distributions following excitation of the large R_B Rydberg state at 752.2 Å and the valley next to this peak. Ionization in the valley strongly favors direct ionization.

peaks. This distribution corresponds most closely to that expected from direct ionization.

The distribution of ejected electron energies in Figs. 6 and 7 can be interpreted in terms of the Bardsley–Smith[18,19] model of autoionization. For long lived autoionizing states for which the lifetime is larger than the vibrational period, and the molecule is excited at the maximum of the resonance, the distribution of final vibrational states is given by the relation[20]

$$\frac{\sigma_\alpha}{\sigma_c} = F^2_{i\alpha} + F^2_{v\alpha}\left[\frac{\sigma_v^{\max}}{\sigma_c} - 1\right], \qquad (2)$$

in which the F^2's are the Franck–Condon factors, and the subscripts, i, v, and α are the vibrational quantum numbers of the initial ground state, the autoionizing state, and the final ion state, respectively. The partial cross sections σ_α, for exciting the vibrational ionic states α, is a function of $\sigma_v^{\max}$ and σ_c, the photoionization cross sections on top of the resonances and in the valleys where it is assumed to be equal to the direct photoionization cross section. The two terms in Eq. (2) represent contributions from direct and autoionization, respectively. In the case of ionization to the $\tilde{X}$ state of CO_2^+, direct ionization contributes mainly to the formation of the ion in the ground vibrational state. This model has been tested most recently by Guyon and Ferreira[21] in the case of autoionization in O_2^+. In its application to the data of Figs. 6 and 7, we assume that the geometry of the $\tilde{A}$ Rydberg states is the same as that of the CO_2^+ $\tilde{A}$ state, so that the known Franck–Condon factors[22,23] between the CO_2^+ $\tilde{A}$ and $\tilde{X}$ states can be used to calculate the final state vibrational distribution. The intensities of the predicted ion vibrational states are shown as lines in Fig. 6.

Although the PES is not sufficiently resolved to claim quantitative agreement between the Bardsley–Smith model and the data, the qualitative features of the data are clearly reproduced in the calculation. The spectra obtained for $n = 4$ and $n = 5$ and the same initial v_1 level, show almost the same distributions. The fact that the latter look narrower results from the TOF method of electron energy analysis. We draw the following conclusion on the basis of this agreement. The intense Rydberg peaks belong to states that are coupled primarily to the $^2\Pi_g$ $\tilde{X}$ ground state ionization continuum. As a result, only the ν_1 symmetric stretch is excited in the autoionization process. It is unfortunate that the energy resolution of the PES in Fig. 6 does not allow us to claim that the bending modes are not excited.

In contrast to the good agreement between the Bardsley–Smith model and the experimental results for the sharp $\tilde{A}$ state Rydberg states, the model does not work for the largest of all of the peaks. This is the $B_4s(000)$ state at 752.2 Å, the lowest member of the Rydberg series converging to the $\tilde{B}$ state of CO_2^+. Because the geometry of the CO_2^+ $\tilde{B}$ state is similar to that of the ground CO_2 and CO_2^+ states, ionization at 752.2 Å should result in the formation of primarily $\tilde{X}$ (000) state ions. The spectrum in Fig. 7 has the large (000) peak, but in addition indicates that CO_2^+ ions are formed in a broad distribution of internal energies, quite different from that expected on the basis of the Franck–Condon factors. This shows that the $B_4s(000)$ peak is not a pure Rydberg state, but is strongly perturbed by neighboring states. Indeed, its exceptional height itself suggests the same conclusion.

2. Resonance autoionization (770–830 Å): Indirect autoionization

There are two questions that arise in connection with the TPES structure from 770 to 830 Å. First, is the observed structure reflecting the distribution of ionic states, or is it correlated with autoionizing neutral states and therefore a reflection of the absorption spectrum? Secondly, what ion states are actually produced?

The answer to the first question is easily obtained by comparing the structure of the PIE and TPES. This examination shows that nearly all of the weak autoionizing peaks in the PIE are associated with peaks in the TPES, thereby demonstrating that the observed TPES structure is associated with autoionizing neutral states. The identity of the kind of ion states formed is less easily determined.

The ion states ultimately formed by autoionization can be one of two types. They may be part of a new electronic state of CO_2^+, for instance, one whose transition probability is relatively high for threshold ionization and would therefore be observed in a TPES but not in a normal PES. The other possibility is that high vibrational levels of the ground electronic state are formed. *Ab initio* calculations[24–27] have not revealed any new electronic states in this energy region, so that the ion states are almost certainly vibrationally excited $\tilde{X}$ state ions. The density of vibrational states at 1.6 eV above the CO_2^+ ($\tilde{X}$) state is about 1 state/meV which is suffi-

ciently high so that an ion state is always within 1–2 meV of the Rydberg state.

The conclusion that vibrationally excited ground electronic state ions are formed in this Franck–Condon gap region is supported by the electron time-of-flight distribution shown in Fig. 8. This spectrum was obtained with an earlier version of the TOF cell[8] consisting of a 5 mm acceleration and a 10 mm drift region. A 1 V/cm electric field extracted the electrons. Under these conditions, initially zero energy electrons are collected with very high efficiency compared to the energetic ones. The spectrum from 0 to 0.2 eV, normalized to the electron collection efficiency, is also shown in Fig. 8. The structureless electron energy distribution at low electron energies indicates that ions are formed in a quasicontinuum of states. Since the dissociation continuum of the CO_2^+ ion begins only at 650 Å (19.07 eV), the only ionization continuum in the 800 Å region is the quasicontinuum of densely spaced vibrational levels of the CO_2^+ ionic ground state.

Even a cursory inspection of the PIE and TPES scans in Fig. 5 shows that the production of threshold electrons is evidently favored in the autoionization of the weak PIE above 790 Å. This tendency can be expressed quantitatively. By normalizing the PIE and TPES at the ionization threshold, where only low threshold electrons are produced, it is possible to determine the fraction of threshold electrons that are formed at any wavelength. Thus the strong autoionizing peak at 765 Å produces only 0.1% threshold electrons. Most of the rest are electrons of about 2.4 eV associated with the lowest vibrational levels of CO_2^+. In contrast, the weak autoionizing peak at 795.76 Å decays with a production of about 8% threshold electrons! How large this fraction is, can be appreciated by the following consideration. The total energy at 795.76 Å is 1.8 eV above the ionization threshold. If the electrons were distributed with equal probability at all electron energies, less than 0.6% of the electrons would have fallen into the 10 meV bandpass of the threshold electron analyzer. We conclude that the electron energy distribution is bimodal. A significant fraction is formed at low energy, while the rest are those of high energy. This conclusion is confirmed by the measured electron time-of-flight distribution (Fig. 8) taken at a photon wavelength of 816.7 Å, on top of one of the TPES peaks. About 16% of the electrons have an energy less than 0.1 eV, while more than 70% have 1.5 eV and correspond to low vibrational levels of CO_2^+.

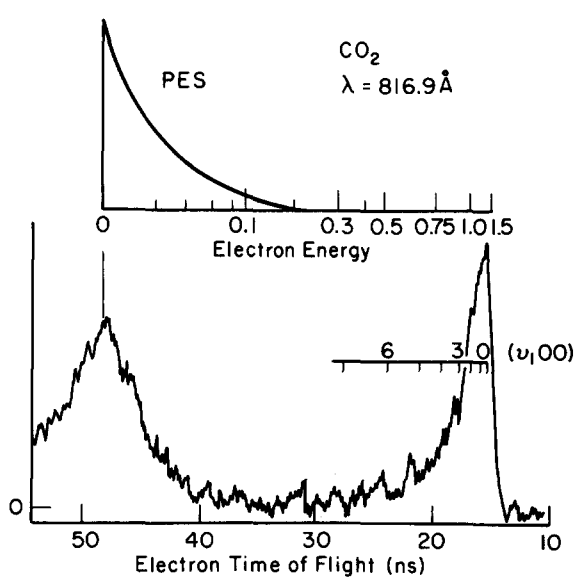

FIG. 8. Electrn TOF distribution and normalized PES at an excitation wavelength of 816 Å.

The electron energy distribution of Fig. 8 is similar to that observed in the analogous $\tilde{X}$ to $\tilde{A}$ Franck–Condon gap region of N_2O^+[8,28] and COS^+,[29] and is characteristic of resonance autoionization. The latter differs from the direct autoionization discussed in connection with the strong autoionization peaks in that it involves several intermediate states so that threshold electrons are proudced via an indirect process. The model developed[28] to explain the production of these vibrationally excited ions in the Franck–Condon gap involves the participation of dissociative neutral valence states as well as vibrationally excited Rydberg states. It was proposed that the conversion of electronic energy into vibrational energy comes about (see Fig. 9) either through a curve crossing of the dissociative states to lower lying autoionizing Rydberg states from which the molecule can autoionize, or by autoionization during the dissociation.

The initial or doorway states in Fig. 9 are ones that carry the oscillator strengths for excitation from the neutral ground state molecule. These are either the quasibound R_A Rydberg states, or the dissociative valence states, labeled D. The final states are the continua associated with the neutral dissociation products and the molecular ion plus its electron.

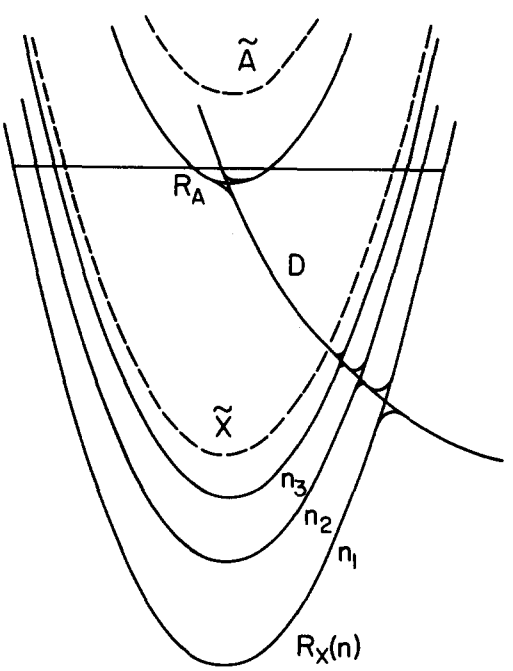

FIG. 9. Model for the low energy electron production and dissociation to neutral products. R_A is a Rydberg state converging to the ion state $\tilde{A}$ and D is a neutral dissociating state. Both of these states can be reached from the ground state molecule. The D state couples the R_A and R_x states. The latter are Rydberg states converging to the ground ionic state. Autoionization of the R_x states leads to low energy electrons that are associated with vibrationally excited $\tilde{X}$ state ions.

The intermediate states important for threshold electron production are the high vibrational levels of the Rydberg states $R_x(n,v,j)$ that converge to vibrationally excited ions and whose energy falls within the resonance width ΔE.

All the states of the same parity are coupled by homogeneous coupling matrix elements and the relative coupling strengths determine the decay mode of the initially prepared doorway state. For instance if the coupling between the Rydberg and final ion state $V(R_A,X)$ is much stronger than with the dissociative state $V(R_A,D)$, the R_A state will decay by a direct autoionization process as described by the Bardsley–Smith model. This situation is, in fact, observed in the strong R_A states converging to the $\tilde{A}$ state of CO_2^+.

Strong predissociation to neutral products dominates following excitation of the D states when the dissociative valence state interacts weakly with the ionization continuum, $V(D,X) \sim 0$. Similarly strong dissociation of the $\tilde{A}$ Rybergs states will take place if $V(R_A,D)$ is large. This will show up in the difference between the total ionization and absorption cross sections. If, on the other hand, $V(D,X)$ is large, so that the autoionization rate is much greater than the vibrational frequency, then ionization of the D state will take place prior to any nuclear motion. The photoionization cross section will be enhanced by the contribution of the D state absorption, but the final vibrational state distribution will approximate that for direct ionization.

The situation relevant for the production of threshold electrons by resonance autoionization arises when the couplings among the states are in an intermediate range. Specifically, when $V(D,X) \sim V(D,R_x) \sim V(R_x,X)$, the initial excitation to the dissociative D state will indirectly populate the high vibrational levels of the R_x states. These Rydberg states are now coupled to the ionization continuum via two competitive pathways. They can either cross back to the D state and ionize with a broad distribution of electron energies, or they can ionize directly from the R_x state via mixing of vibrational (nuclear) and electronic motion. This non-Born–Oppenheimer, vibrational autoionization is expected to produce low energy electrons because of the $\delta v = -1$ propensity rule of Berry and Nielson.[30]

The above mechanism for the production and autoionization of the vibrationally excited R_x states depends on the multidimensionality of polyatomic species. A large density of rovibrational states is required to ensure near resonance with the initially excited doorway states. Equally important is the dephasing of the vibrational modes after the D to R_x crossing which prevents the molecule from passing immediately back to the D state to decay by the more rapid electronic autoionization or dissociation. Thus, in diatomics, such as NO that are also predissociated by a repulsive valence state,[31] the distribution of electron energies is broad and is not peaked near zero energy.

Vibrational autoionization in polyatomics is expected to be greatly enhanced for high energy levels of the bending vibrational mode since the autoionization rate is proportional to the ratio $(v+1)/w$, where v is the vibrational quantum number and w is the bending frequency.[21] Although the vibrational autoionization model favors the production of low energy electrons,[28] it alone cannot explain quantitatively the sharp peak at zero energy in the electron energy distribution of Fig. 8. However, recent work of Chupka *et al.*[32] has shown that the inclusion of rotational autoionization in the model leads to PES that are sharply peaked at zero energy.

One of the major pieces of evidence supporting this model for resonance autoionization comes from the similarity of the fluorescence excitation cross section for neutral dissociation fragments and the TPES in the case of N_2O[28] and COS.[29] Such a correspondence between neutral fragment fluorescence excitation spectrum and the TPES exists also in CO_2. Gentieu and Mental[17] have monitored the fragment CO $\tilde{A}$ state emission as a function of the exciting wavelength. This excitation spectrum is very similar to the TPES in Fig. 5, showing both the broad hump between 750 and 830 Å and the enhancement of the autoionization peaks in the region 791 to 820 Å. For instance, the peaks at 802 and 796 Å are twice as high as the broad background in both the TPES and the fluorescence excitation spectrum, while they are barely visible in the total ion spectrum.

The model embodied in Fig. 9 accounts for the pronounced structure observed in the TPES. That is, the broad background in the PIE contributes relatively little to the TPES, while the peaks yield between 5% and 8% threshold electrons. The more obvious structure in the TPES compared to the PIE makes possible a more certain identification of these autoionizing states. The spacing of the peaks near 820 Å corresponds to the excitation of a bending mode. This suggests that absorption is taking place to a bent valence state. The existence of such states has been proposed on the basis of several calculations,[16,25] but they have never been observed. In addition to this series of peaks with excitation of the ν_2 mode, there is another series with spacings that correspond to the excitation of the symmetric stretch. This spacing is similar to that found in the $\tilde{A}$ ionic state so that this is probably a Rydberg state converging to the CO_2^+ $\tilde{A}$ state. Table II lists the wavelengths, energies, and our assignments for these TPES peaks.

If we take the vibrational origin of the Rydberg peaks at 816.8 Å, the principal effective quantum number n^* can be calculated to be 2.5 from the Rydberg formula $E_r = \text{I.P.}(\tilde{A}) - R/n^{*2}$, in which R is the Rydberg constant and E_r is the energy of the Rydberg state. The next Rydberg state, which should have an effective quantum number of $n^* = 3.5$ should lie at around 764 Å. This is a region in which there are many unassigned peaks, a number of which seem to follow a similar pattern as the $n^* = 2.5$ series. However, they are weak and are not easily seen in the presence of the much stronger major series.

The assignments of the TPES peaks to the various vibrational modes in the CO_2 Rydberg states is based mainly on the energies of these states and the expectation of simple progressions. Attempts to fit the peaks to combination bands of a single electronic state (rather than the two proposed), were successful only when the presence of such states as (290) and (170), and the absence of such states as (160) and (100) were assumed. Such anomalies forced us to propose the excitation to two states. Unfortunately, the signal-to-noise ratio of the $^{12}CO_2^+$ and the $^{13}CO_2^+$ data in this wavelength region was insufficient to determine isotope shifts in

TABLE II. $^{12}CO_2$ PIE and TPES wavelengths and energies in Franck–Condon gap.

PIE Å				
This work	McCulloh[a]	TPES (Å)	Vibrational energy (cm^{-1})[b]	Assignment
827.9	827.5	827.8	0	$V(000)$
824.6	824.1	824.5	484	$V(010)$
821.1	820.3	821.0	1000	$V(020)$
		817.5	1522	$V(030)$
816.9	816.6	816.8	0	$R(000)$
	814	814.3	2003	$V(040)$
811.5		811.2	2472	$V(050)$
809.6	809.4	809.6	1090	$R(100)$
807.3	807	807.9	2976	$V(060)$
804	804			$V(070)$?
		802.4	2197	$R(200)$
800.8	800.8	801.2	4010	$V(080)$
		797.3	4590	$V(090)$
796.2	796.6			
		795.8	3230	$R(300)$
794.8	795			
		794.7	5032	$V(0\,10\,0)$
		789.5	4233	$R(400)$
		782.4	5382	$R(500)$
		776.1	6420	$R(600)$

[a] Reference 15.
[b] The vibrational energy is based on the two origins, one for the valence state, the other for the Rydberg state.

the energy positions of the various peaks.

C. Region of the $^2\Pi_u(\tilde{A})$ state

1. Progression in ν_1 and associated hot band structure

Figure 10 shows the $^{13}CO_2$ and $^{12}CO_2$ TPES in the region of the $\tilde{A}$ and $\tilde{B}$ states of CO_2^+. The spin orbit splitting in this state is much less (97 cm^{-1}) than in the ground ionic state so that our energy resolution is insufficient to split the peaks in the TPES. The fact that the previously published TPES of Frey *et al.*[5] clearly shows the splitting demonstrates the superior resolution of this earlier study. On the other hand, the signal-to-noise ratio of the present study is considerably better which makes possible the deconvolution of the spin orbit peaks as shown by the dashed lines in the figure. The major series of peaks is the one formed by the successive excitation of the symmetric stretching frequencies ν_1.

The TPES is similar to the HE (1) PES in the low energy region of the $\tilde{A}$ state. The dominant peaks belong to the series $(v_1 00)v_1 = 0, 1, 2$. Each of these has a weak shoulder on the low energy side of the peak. The origin of these shoulders has been interpreted differently by the authors of several PES studies. Potts and Fattahallah[3] as well as Reineck *et al.*[1] claim that they result from a hot band absorption in which one quantum of the bending vibration originally in the CO_2 molecule remains in the ion. Because the frequency of the

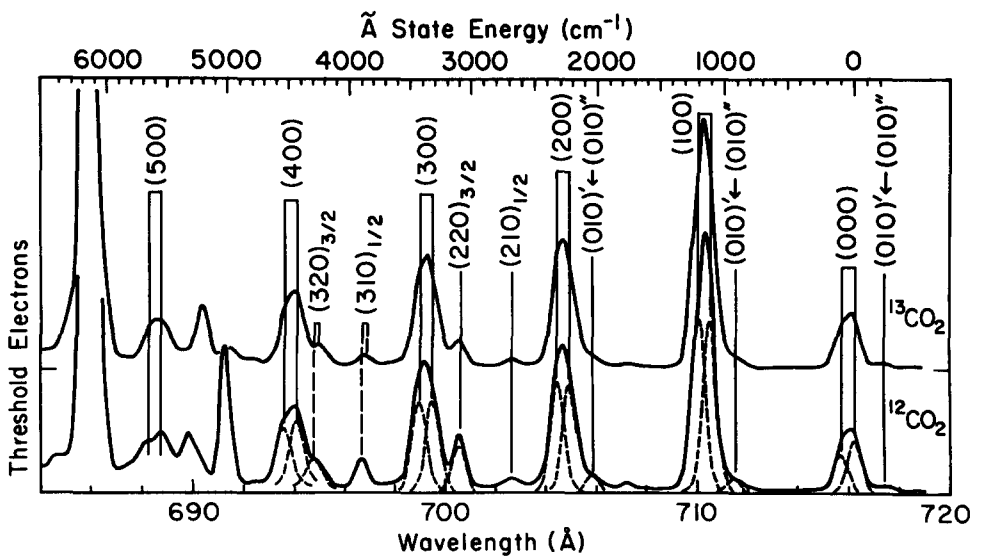

FIG. 10. TPES of $^{12}CO_2$ and $^{13}CO_2$ of the $\tilde{A}$ state. The latter spectrum has been shifted so that the (000) levels of the two spectra are superimposed.

ionic mode is reduced from the 667 cm^{-1} value in CO_2 neutral to 460 cm^{-1} in the ion, this hot band shows up as a shoulder centered about 220 cm^{-1} to the low energy side of each of the (v00) peaks. Kovac,[4] on the other hand, interprets the shoulders on the (v00) peaks as doubly excited ν_2 modes. Unfortunately, the derived value for the ν_2 frequency is nearly the same for the two interpretations. Potts and Fattahallah[3] obtain 467 cm^{-1} and Reineck *et al.*[1] report 484 ± 40 cm^{-1} assuming hot band structure, while Kovac obtains a ν_2 of 480 cm^{-1}.

The shoulders are clearly evident in the TPES spectrum of Fig. 10 for the $\nu_1 = 0$, 1, and 2 peaks. The shoulder on the (000) peak can only come from a hot band contribution. If the shoulders on the other two peaks were assigned to (020) and (120) excitations, these peaks would show an isotope shift of -27 cm^{-1}, while a hot band assignment would predict a shift $+6$ cm^{-1}. In fact, these two shoulders do not shift, which is within the experimental error of 10 cm^{-1}, consistent with the hot band assignment. Finally, the intensity of 3% is in reasonable accord with the expected Boltzmann intensity of 3.7% for a gas at 300 K. The ν_2 values derived on the basis of hot band structure are 466 and 454 cm^{-1} for $^{12}CO_2^+$ and $^{13}CO_2^+$, respectively, which agree very well with the $^{12}CO_2^+$ value of 460 cm^{-1} obtained by Gauyacq *et al.*[11] on the basis of the high resolution emission spectroscopy.

2. Autoionization and the $\tilde{A}$ state TPES

The TPES at the higher energies of the $\tilde{A}$ state becomes more complicated. There are peaks of significant intensities that cannot be assigned to hot bands or obvious combination bands. Some of the peaks above the (200) level appear about halfway between the ($v_1$00) states while the rest appear as shoulders on the low energy side of the ($v_1$00) peaks. These peaks could be assigned to ($v_1$10) and ($v_1$20) vibrations from which we would derive ν_2 frequencies of 472 ± 20 (^{12}C) and 468 ± 25 (^{13}C) cm^{-1}. However, there are several problems with this interpretation. First of all, the scatter in the values determined from the several peaks is more than seems reasonable. Secondly, the ($v_1$10) and ($v_1$20) states should be split by both spin orbit and Renner–Teller interactions. Both of these effects are about half as strong in the $\tilde{A}$ state as they are in the $\tilde{X}$ state. Nevertheless, these peaks should be at least as broad as the ($v_1$00) peak whose width of 185 cm^{-1} is a result only of spin orbit splitting. Yet, several of these extra peaks are only 110 cm^{-1} wide which is essentially our resolution of 100 cm^{-1}. Therefore, these peaks cannot be assigned to the unresolved cluster of ($v_1$10) or ($v_1$20) states. Rather, they must be assigned to only a single component of these states. Because these peaks in the TPES are not present in the He(I) PES, they must derive their intensity through an autoionization process.

The energy region between the $\tilde{A}$ and $\tilde{B}$ contains a large number of autoionizing levels. The major series is the one that converges to the $\tilde{B}$ state. In addition, each of the $\tilde{A}$ state vibrational levels has several Rydberg series. As a result, there are many overlapping absorption peaks that are not resolved. Although the TPES peaks in Fig. 10 do not correspond precisely to autoionization peaks, they do fall on the shoulders of a number of them. It appears that certain specific Rydberg states decay in such a manner as to form ions of the same energy with the production of zero energy electrons. Thus the position of the TPES peaks are determined not only by the ion energy, but by the presence of an appropriate Rydberg state as well. For this reason it is possible to have TPES peaks for only one of the spin orbit components of the (310) and the other spin orbit component of the (320) pair.

3. New sharp autoionization features revealed by TPES

The most remarkable aspect of the TPES in the region of the CO_2^+ $\tilde{A}$ state is the peak at 691.25 Å in the $^{12}CO_2^+$ spectrum, which was also observed in the $^{12}CO_2$ TPES by Batten *et al.*[7] and Frey *et al.* This peak, and its companion at 689.85 Å, are absent in the $^{13}CO_2^+$ TPES. Instead, there is a single peak which is in turn absent from the $^{12}CO_2^+$ TPES. The magnitude of the shifts are beyond any that can be expected on the basis of isotope shifts. These peaks, which are not observed in the He(I) PES studies,[1–4] result evidently from autoionization process. We performed a series of complimentary experiments in order to determine the natures of the autoionizing precursor and the final ionic states.

The width of the new state is considerably smaller than the width of even the narrowest normal TPES peaks. A high photon resolution TPES scan revealed that the peak widths were determined exclusively by the photon bandwidth (5 meV) and not by the electron energy analyzer bandpass. This might suggest that we are simply exciting an autoionizing state. However, we verified that the maxima in the TPES did not correspond to any sharp autoionizing features observed in the total PIE, so that these TPES peaks correspond to specific states of CO_2^+, produced in a narrow energy distribution. This was confirmed by the observation, based on several electron TOF distributions in the vicinity of these peaks, that these CO_2^+ states were formed over a narrow band (1–2 Å) of photon excitation energies, but at specific ion energies.

The fact that these peaks are observed at ion energies which do not match any combination of bands of the A state and are not correlated in the isotopic spectrum, suggests that these transitions are due to accidental perturbations, possibly between some particular $\tilde{A}$ state rovibrational levels and another electronic state of CO_2^+. Such an interpretation is supported by the experiments of Schlag *et al.*,[33] who noted the anomalously long radiative lifetime of 165 ns for the state at 691.25 Å, compared to the lifetimes of 106 ± 10 ns for the other $\tilde{A}$ state vibrational levels.

The long radiative lifetime as well as the calculations of Praet *et al.*,[24] leads us to conclude that the pertubing state is a quartet state. The calculations predict an energy of about 21 eV for such a state in the linear ($^4\Pi_u$) configuration, but a much lower energy as the ion bends. The energy of the bent $^4B_1$ ground state is calculated to be just slightly above the $\tilde{A}$ $^2\Pi_u$ (000) level so that it is energetically capable of perturbing the $\tilde{A}$ state levels. Because only a few of the $\tilde{A}$ $^2\Pi_u$ and $\tilde{a}$ $^4B_1$ state vibrational and rotational levels are likely to have the appropriate energy for interacting, rather different

$^{12}CO_2^+$ and $^{13}CO_2^+$ states are expected to be perturbed, as is experimentally found.

There remains still the question of how these extra states are produced. Because they are only seen in a narrow photon range of a few angstroms, suggests that they result from the autoionization of one or two broad states. A reasonable candidate for this autoionizing state is a Rydberg state that converges to the $\tilde{C}$ state, and which is characterized by a very broad resonance (see the 650–680 Å ion signal in Fig. 3). The $n = 3$ members of these series are not observed since they are diffuse and expected to fall among the strong $\tilde{A}$ and $\tilde{B}$ Rydberg states at 734 ($\delta = 0.67$), 721($\delta = 0.5$), and 695.6 Å($\delta = 0.05$). Among them, the $\delta = 0.05$ $n = 3$ member is expected to be sufficiently broad to encompass the energy region in which we observe the extra TPES peaks.

The preferential ejection of low energy electrons suggests that autoionization to this mixed ionic state proceeds by a mechanism similar to the one described in Fig. 9. In this case, the initial excitation could be to R_C ($n = 3$). This state is almost certainly coupled to one of several R_a Rydberg states converging to the bent $\tilde{a}\ ^2B_1$. Praet *et al.*[24] have shown that the ionic quartet state predissociates the $\tilde{C}$ state. Thus, it is certainly likely that a similar interaction takes place with the corresponding Rydberg states. In fact, the fluorescence excitation spectrum of Gentieu and Mentall[17] demonstrates that neutral dissociation channels are still strong in this energy region. In summary, the unexpected states may be mixed $\tilde{A}\ ^2\Pi_u$ and $\tilde{a}\ ^4B_1$ levels of which there are only a small number because of the energy matching requirement. These states can only be reached via an autoionization mechanism since their bent geometry causes the Franck–Condon factors for direct ionization to be extremely small.

D. TPES of the $^2\Sigma_u(\tilde{B})$ state

Figure 11 shows the expanded version of the $\tilde{B}$ state TPES for $^{12}CO_2$ and $^{13}CO_2$. This region of the TPES consists of a number of $\tilde{B}$ and high energy $\tilde{A}$ state peaks. These peaks have been carefully sorted out in a recent high resolution PES study of Wannberg *et al.*[2] However, the higher energy region of the spectrum is so congested that no individual peaks could be identified. Nevertheless, the envelope of peaks was successfully fitted with a large number of peaks consisting mostly of combination bands.

The only frequency that can be easily determined from the PES is ν_1, which is 1280 ± 10 cm^{-1}. The asymmetric stretching mode is only weakly excited and lies among a number of combination bands. As a result, there is no agreement concerning its value. Wannberg *et al.*[2] deduced a ν_3 frequency of 1855 cm^{-1}, which differs considerably from the earlier value of 2365 cm^{-1} of Potts and Fattahallah.[3] On the other hand, the ν_2 frequency for the $\tilde{B}$ state is known very well from the high resolution fluorescence spectra of Gauyacq *et al.*[11]

The TPES differs from the PES in that certain of the peaks are greatly enhanced so that the TPES is considerably less congested than the PES. In addition, the isotope shifts are again an important aid in assigning the peaks. A particularly large shift occurs in the (440) $\tilde{A}$ peak. The identification of the (010) peak is thwarted by the strong (600) $\tilde{A}$ peak so that we cannot confirm the fluorescence measurements. On the other hand, the energy of the (100) $\tilde{B}$ peak falls at 1270 and 1272 cm^{-1} for the two spectra. This peak is so strong, isolated, and sharp that we tend to favor it over the 1280 value generally agreed upon. Batton *et al.*[7] also reported a low value of 1274 cm^{-1}.

The TPES has three peaks that appear to be associated with the elusive ν_3 mode. These are the (101), (002), and (102) peaks which have appropriately large isotope shifts. From these three peaks, we deduce the ν_3 frequencies of 1820 ± 15 and 1775 ± 15 cm^{-1} for $^{12}CO_2^+$ and $^{13}CO_2^+$, respectively. This shift of 45 cm^{-1} is close to the predicted shift of 52 cm^{-1}. These ν_3 values are definitely to be preferred over the Potts and Fattahallah value of 2365 cm^{-1}. We see

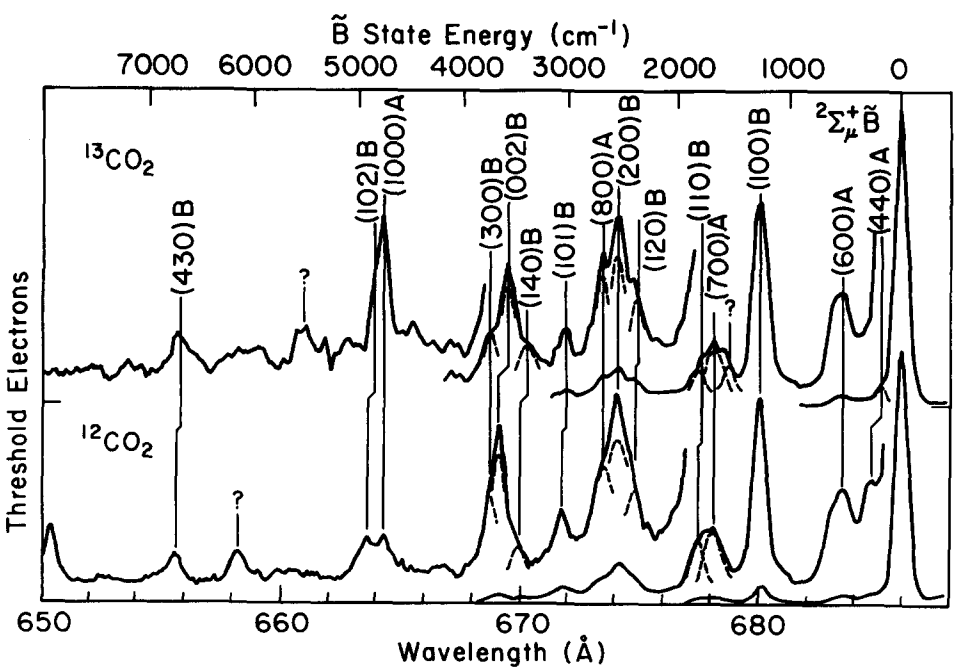

FIG. 11. TPES of $^{12}CO_2$ and $^{13}CO_2$ of the $\tilde{B}$ state. The latter spectrum has been shifted so that the (000) levels of the two spectra are superimposed.

no evidence for a $2\nu_3$ peak at 4730 cm^{-1}. From the lack of an isotope shift, our peak at 4750 cm^{-1} can be assigned rather confidently to the (10 0 0) vibrational level of the $\tilde{A}$ state.

E. TPES in region of the O^+ onset

The onset of 19.071 (650.1 Å) for the dissociation to O^+ (^4S) + CO ($^1\Sigma^+$) lies below the $\tilde{C}$ (000) state. There are no PES peaks in this Franck–Condon gap region. However, it is evident from Fig. 12 that there are threshold electron peaks. The PIE scan exhibits three Rydberg series that converge to the CO_2^+ $\tilde{C}$ state. The assignments along with the energy defects are shown in Fig. 12. We have also included the O^+ signal measured by Eland and Berkowitz.[34] The wavelength scales of the TPES and the PIE scans have been precisely matched by equating the energy of the TPES $\tilde{C}$ state with the extrapolation of the Rydberg series.

Since the region below the $\tilde{C}$ (000) limit is a Franck–Condon gap, production of low energy electrons associated with excited ions, and therefore O^+ fragment ions, must result from an autoionization process. This is quite apparent when one compares the CO_2^+ and O^+ PIE curves in which the window resonances associated with the R_C ($\delta = 0.51$) Rydberg series appear as sharp peaks in the O^+ PIE curve. However, there appears to be no simple correspondence between the production of threshold electrons and excitation of any particular Rydberg series. For instance, the TPES peak at 658.35 Å coincides with $\delta = 0.05$, $n = 5$ Rydberg state; yet there is only a hint of a TPES peak for the $n = 6$ Rydberg state and nothing at all for $n = 7$ and 8. A similar inconsistency exists for the other two Rydberg series. At 655.72 Å the $\delta = 0.67$, $n = 6$ Rydberg peak coincides with a TPES peak, while the higher members of this series have no associated TPES peaks. It is particularly striking that the $^{12}CO_2$ and $^{13}CO_2$ TPES peaks do not coincide in this region. In fact, there are no peaks in the $^{13}CO_2$ TPES between 655 and 640 Å, and the major $^{12}CO_2^+$ peak at 650.35 Å has no $^{13}CO_2^+$ counterpart.

Since the formation of O^+ product ions near the dissociation limit must involve the production of low energy electrons, it might be expected that the O^+ PIE curve would follow the TPES. Yet this does not appear to be the case. For instance, the O^+ peak at 649 Å is absent in the TPES. Since this energy is just 33 meV above the dissociation onset, the energy of the ejected electron must be between 10 and 33 meV. In addition, the $^{12}CO_2^+$ and $^{13}CO_2^+$ PES show marked differences. In fact, since there is no peak in the $^{13}CO_2$ TPES at 650 Å we conclude that a O^+ PIE from $^{13}CO_2$ would not show an onset at the thermochemical limit.

A number of the autoionization characteristics in this energy region are similar to the ones mentioned in connection with the formation of the extra peaks in the $\tilde{A}$ state region. That is, only a few states are formed, the effect of ^{13}C isotopic substitution is dramatic, and the dissociative channel as exhibited by the fluorescence excitation spectrum of Gentieu and Mentall[17] is still present, although very weak. In addition, the same R_C Rydberg states may be involved. These facts point to a similar mechanism for the production of low energy electrons and vibrationally excited ions.

F. TPES of the $^2\Sigma_g^+$ $\tilde{C}$ state

The final TPES band is that of the CO_2^+ $\tilde{C}$ state, which is shown in Fig. 13. As in the previous bands, we see the shifts associated with the ^{13}C isotopic substitution. This is particularly advantageous in this band, because of the considerable controversy concerning the ν_3 frequency. The ν_2 and ν_1 frequencies are well established, although the origin of the strong (010) excitation which is formally forbidden, is not certain. The TPES in Fig. 13 supports these previous conclu-

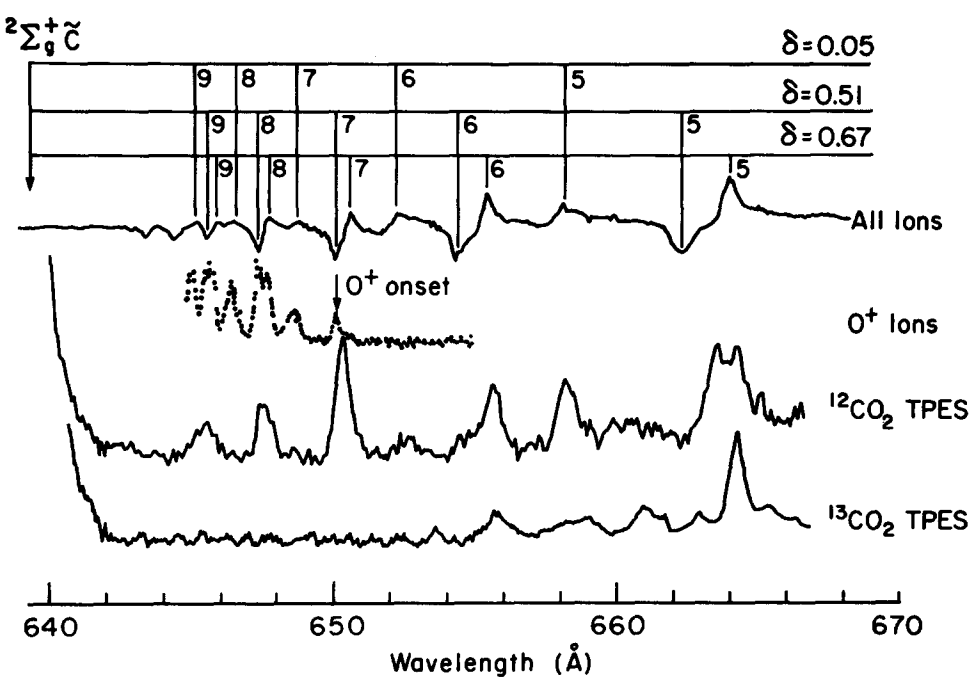

FIG. 12. TPES and PIE in the region of the O^+ dissociation onset just below the $\tilde{C}$ state. The O^+ PIE is taken from Eland and Berkowitz (Ref. 34).

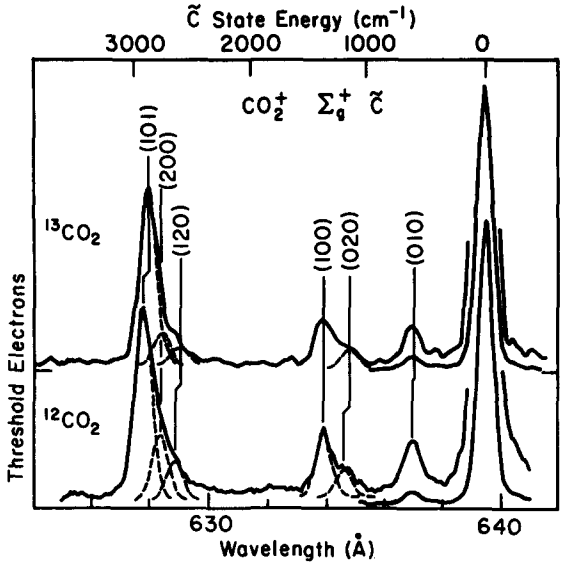

FIG. 13. TPES of $^{12}CO_2$ and $^{13}CO_2$ of the $\tilde{C}$ state. The latter spectrum has been shifted so that the (000) levels of the two spectra are superimposed.

sions. The (100) band does not shift upon isotopic substitution, while the bending frequency is shifted.

The peak near 2800 cm^{-1} is considerably more complicated. Two of the components can be attributed to the (200) and (120) overtone and combination bands. However, the major peak at 2930 cm^{-1} has been interpreted in three different manners. Kovac[4] attributed this peak to the (001) mode thereby reporting a ν_3 frequency of 2960 cm^{-1}. Potts and Fattahallah[3] on the other hand claimed that this peak is due to (011) combination band from which they derive a ν_3 frequency of 2345 cm^{-1}. Finally, Reineck *et al.*[1] attributed this peak to a (101) mode and derived a ν_3 frequency of 1524 cm^{-1}. In principle, we should be able to distinguish the Reineck assignment from the other two by use of the isotope shift. Both the (011) and the (001) assignments would result in an isotope shift of about 84 cm^{-1}, while the (101) assignment would imply a shift of 44 cm^{-1}. On the basis of the observed shift of 55 cm^{-1}, we favor the Reineck assignment and derive a ν_3 frequency of 1530 cm^{-1}.

The argument for the (101) assignment on the basis of the isotope shift must be tempered somewhat because of the anomalous intensity of this peak. This intensity is certainly derived from a perturbation with neighboring states. As a result, the intensity as well as the peak position could be affected. Because the strength of the pertubation is dependent on the energy differences, it may well be that the $^{12}CO_2^+$ and the $^{13}CO_2^+$ ν_3 peaks are shifted by different amounts.

A number of older PES scans of the CO_2^+ $\tilde{C}$ state exhibited a peak at about 2400 cm^{-1}. This has been demonstrated[1,3] to be the result of an inelastic scattering of the photoelectrons with CO_2 molecules in the pressurized cell. Excitation of the (001) mode in CO_2 would lead to an electron peak shifted in energy from the (000) peak by the neutral CO_2 frequency. Although our cell pressure is considerable ($\sim$0.001 Torr) so that such inelastic collisions certainly take place, they do not affect the TPES except perhaps to reduce the signal.

IV. CONCLUSION

Analysis of the high resolution threshold photoelectron spectra of isotopically substituted $^{12}CO_2$ and $^{13}CO_2$ has provided new and detailed information on the spectroscopy of the molecular ions, and on the mechanism for photoionization.

The adiabatic ionization potentials of $\tilde{X}$, $\tilde{A}$, $\tilde{B}$, and $\tilde{C}$ states have been determined within 2 meV, and some of the vibrational frequencies for these states have been determined with better accuracy than in previous publications as shown by the consistent agreement with optical data of Gauyacq *et al.*[11] and Larcher.[12] The controversies over the ν_3 asymmetric stretching frequencies for the $\tilde{B}$ and $\tilde{C}$ states appear now to be settled with the values of $\nu_3(\tilde{B}) = 1820 \pm 10$ cm^{-1}, and $\nu_3(\tilde{C}) = 1530 \pm 10$ cm^{-1}.

The resonance autoionization mechanism responsible for the production of threshold electrons in the Franck–Condon gap regions of polyatomic molecular ions was investigated in detail. As proposed previously for autoionization in N_2O, and now confirmed for the case of CO_2, the role of neutral valence states is important in the generation of threshold electrons. The analysis of the TPES in the $\tilde{A}$ state region and below the $\tilde{C}$ state indicates that resonance autoionization takes place at elevated energies as well. On the basis of the dramatic isotope effect, the narrow TPES peak width, and the long radiative ion lifetime measured by Schlag *et al.*,[33] we conclude that the resonance autoionization populates states that have some quartet character. This conclusion is consistent with recent calculations of the $\tilde{a}\ ^4B_1$ state by Praet *et al.*[24]

ACKNOWLEDGMENTS

We thank our colleagues: Odile Dutuit, Jacque Delwiche, M. J. Hubin-Franskin, Tom Govers, Horst Frolich, Michel Lavollee, and Martine-Richard Viard for help in running the experiments. We are particularly indebted to Sydney Leach for his encouragements and suggestions and to Joel Rostas and Alberto Beswick for providing us with calculated Franck–Condon factors. We also appreciate the long hours of work offered by the staffs of the Orsay linear accelerator and of LURE in operating the storage ring. This work was made possible by a contract from the French National Research Center (ATP-CNRS), a joint CNRS-NSF grant, as well as an NSF grant.

[1] I. Reineck, C. Nohre, R. Maripuu, P. Lodin, S. H. Al-Shamma, H. Veenhuizen, L. Karlsson, and K. Siegbahn, Chem. Phys. **78**, 311 (1983).
[2] B. Wannberg, H. Veenhuizen, L. Mattsson, K. E. Norell, L. Karlsson, and K. Siegbahn, J. Phys. B **17**, L259 (1984).
[3] A. W. Potts and G. H. Fattahallah, J. Phys. B **13**, 2545 (1980).
[4] B. Kovac, J. Chem. Phys. **78**, 1684 (1983).
[5] R. Frey, B. Gotchev, O. F. Kalman, W. B. Peatman, H. Pollak, and E. W. Schlag, Chem. Phys. **21**, 89 (1977).
[6] R. Stockbauer, Adv. Mass Spectrom. A **8**, 79 (1980).
[7] C. F. Batten, J. A. Taylor, and G. G. Meisels, J. Chem. Phys. **65**, 3316 (1976).
[8] T. Baer, P. M. Guyon, I. Nenner, A. Tabche-Fouheille, R. Botter, L. F. A.

Ferreira, and T. R. Govers, J. Chem. Phys. **70**, 1585 (1979).
[9]D. Field, J. P. Ziezel, P. M. Guyon, and T. R. Govers, J. Phys. B **17**, 4565 (1984).
[10]G. Herzberg, *Molecular Spectra and Molecular Structure. II. Infrared and Raman Spectra of Polyatomic Molecules*, 2nd ed. (Van Nostrand, Princeton, N. J., 1950).
[11](a) D. Gauyacq, M. Horani, S. Leach, and J. Rostas, Can. J. Phys. **53**, 2040 (1975); (b) D. Gauyacq, C. Larcher, and J. Rostas, *ibid.* **57**, 1634 (1979); (c) C. Larcher, D. Gauyacq, and J. Rostas, J. Chim. Phys. (Paris) **77**, 655 (1980).
[12]C. Larcher, These D'Etat, Universite de Paris, Orsay, 1982.
[13]Y. Tanaka and M. Ogawa, Can. J. Phys. **40**, 879 (1962).
[14]G. Herzberg, *Molecular Spectra and Molecular Structure. III. Electronic Spectra of Polyatomic Molecules* (Van Norstrand, Princeton, 1966).
[15]K. E. McCulloh, J. Chem. Phys. **59**, 4250 (1973).
[16]M. Krauss, S. R. Mielczarek, D. Neumann, and C. E. Kuyatt, J. Geophys. Res. **76**, 3733 (1971).
[17]E. P. Gentieu and J. E. Mentall, J. Chem. Phys. **58**, 4803 (1973).
[18]A. L. Smith, Philos. Trans. R. Soc. London Ser. A **268** 169 (1970).
[19]J. N. Bardsley, Chem. Phys. Lett. **2**, 329 (1968).
[20]J. H. D. Eland [J. Chem. Phys. **72**, 6015 (1980)] has reformulated the Bardsley Smith relation to that given by Eq. (2).
[21]P. M. Guyon and L. F. A. Ferreira, Workshop on Atomic and Molecular Autoionization, Argonne National Lab. Ill, 1985, ANL Report PHY 85-3.
[22]J. C. McCallum and R. W. Nicholls, J. Phys. B **4**, 1096 (1971).
[23]A. Beswick and J. Rostas (private communication).
[24]M.-Th. Praet, J.-C. Lorquet, and G. Raseev, J. Chem. Phys. **77**, 4611 (1982); in *Molecular Ions: Geometries and Electronic Structures*, edited by J. Berkowitz and K. O. Groeneveld, NATO ASI Ser. B (Plenum, New York, 1983), Vol. 90.
[25]H. Nakatsuji, Chem. Phys. **75**, 425 (1983).
[26]N. Padial, G. Csanak, B. V. McKoy, and P. W. Langhoff, Phys. Rev. A **23**, 218 (1981).
[27]R. S. Mulliken and W. C. Ermler, *Polyatomic Molecules; Results of ab initio Calculations* (Academic, New York, 1981).
[28]P. M. Guyon, T. Baer, and I. Nenner, J. Chem. Phys. **78**, 3665 (1983).
[29](a) I. Nenner and A. Beswick, *Handbook of Synchrotron Radiation*, edited by G. V. Marr (North-Holland, Amsterdam, to be published), Vol. II; (b) M. J. Hubin-Franskin, J. Delwiche, P. M. Guyon, and I. Nenner, *Molecular Ions: Geometries and Electronic Structures*, edited by J. Berkowitz and K. O. Groeneveld, NATO-ASI Ser. B (Plenum, New York, 1983), Vol. 90.
[30]R. S. Berry and S. E. Nielsen, Phys. Rev. A **1**, 383, 395 (1970).
[31]A. Giusti-Suzor and Ch. Jungen, J. Chem. Phys. **80**, 986 (1984).
[32]W. A. Chupka, P. J. Miller, and E. E. Eyler (to be submitted).
[33]E. W. Schlag, R. Frey, B. Gotchev, W. B. Peatman, and H. Pollak, Chem. Phys. Lett. **51**, 406 (1977).
[34]J. H. D. Eland and J. Berkowitz, J. Chem. Phys. **67**, 2782 (1977).